

Towards Prescribed Accuracy in Under-tuned Super-Twisting Sliding Mode Control Loops - Experimental Verification

Dimitrios Papageorgiou¹

Abstract—Obtaining prescribed accuracy bounds in super-twisting sliding mode control loops often falls short in terms of the applicability of the controller in high-performance systems. This is due to the fact that the selection of the controller gains that are derived from the conditions for finite-time convergence may be too restrictive in connection to actuator limitations and induced chatter. Previous work has shown that in case of periodic perturbations, there can be a systematic selection of much lower controller gains that guarantees boundedness of the closed-loop solutions within predetermined accuracy bounds. This study presents an experimental validation of these findings carried out on a commercial industrial motor system.

I. INTRODUCTION

Variable-Structure Control (VSC) and in particular Sliding Mode Control (SMC) techniques [1] constitute a quite attractive family of control strategies due to their inherent robustness against bounded and bounded-rate perturbations. The additional feature of ensuring finite-time convergence has established the use of such algorithms in many fields ranging from aviation and flight control [2] to industrial motion control systems [3], while their application also extends to diagnosis and fault-tolerant control schemes [4]. The need to alleviate the induced chatter in the control signal of the conventional first-order SMC led to the development of second and higher-order SMC laws [5], [6]. Among these, the Super-twisting Sliding Mode controller (STSMC) introduced in [7] and further generalised in [8], has become very popular due to its robust finite-time stabilisation properties and reduced chattering [9].

The simplicity of the STSMC with respect to its design and implementation has motivated a large number of studies on the systematic tuning of the controller. Relating the selection of controller gains to performance specifications is of particular interest since it facilitates easy commissioning of control systems. Despite the “proportional-integral” structure of the controller, the tuning of the STSMC can be challenging and has therefore received significant attention. Closed-form expressions for the controller gains were provided by [10] who used strict Lyapunov functions to prove finite-time stability of the STSMC closed loop. Necessary and sufficient conditions for finite-time convergence were provided in [11] and [12], in which the authors employed geometric arguments relating to the majorant curve contraction requirement. The same conditions were also used to estimate the reaching time as shown in [13]. Tuning rules based on the properties of

limit cycles appearing in linear systems with uncertain actuator dynamics were provided by [14], who used a describing functions framework. Adaptation constitutes an alternative approach to systematic commissioning of STSMC loops. The authors in [15] proposed an adaptive STSMC design for an electropneumatic actuator. A certainty-equivalence adaptive STSMC was presented in [16], where the adaptation was used to avoid unnecessary large controller gains. The authors in [17] and [18] proposed a dual-layer adaptive STSMC for guaranteeing finite-time convergence to the origin for both known and unknown perturbation bounds.

In the majority of the foregoing studies, the selection of the STSMC gains was based on the conditions for finite-time convergence of the error variable to the origin, which require that the integral gain of the STSMC be larger than the bound of the rate of the lumped perturbations affecting the system dynamics [10]. This can be limiting in terms of unrealistically large control signals, especially for application in systems with abrupt-changing perturbations such as Coulomb friction and backlash torques during motion reversals in mechanical systems. However, ensuring finite-time convergence is not necessary for obtaining high accuracy as was demonstrated in [19], where an under-tuned STSMC outperformed several conventional and advanced controllers in a single-axis positioning task. For systems affected by periodic perturbations it was proven [20] that under milder gains conditions compared to those of finite-time convergence, the solutions of the STSMC closed-loop system converge to a limit cycle of the same period as the perturbation. The width of the limit cycle, which is a bound for the control error variable, can be modulated according to prescribed accuracy requirements. The authors provided guidelines for systematic tuning of the STSMC and demonstrated the validity of the method in simulation.

This study pursues experimental verification of the theoretical results presented in [20]. Specifically, a motion control system comprising a commercial Permanent Magnet Synchronous Motor (PMSM) is used as a test platform in a series of experiments proving the existence of stable limit cycles in under-tuned STSMC loops with perturbation-dependent frequency and amplitude characteristics. Moreover, the performance of the closed-loop system is assessed in connection to the tuning method. The remainder of the paper is organised as follows: Section II provides an overview of the theoretical findings in [20]. Section III details the experimental campaign and discusses the results in connection to the theoretical predictions. Finally, conclusions are drawn in Section IV along with some remarks on future work.

¹Dimitrios Papageorgiou is with the Department of Electrical and Photonics Engineering, Technical University of Denmark, Elektrovej 326, 2800 Kgs Lyngby, Denmark dimpa@elektro.dtu.dk

II. OVERVIEW OF THEORETICAL RESULTS

A. Preliminaries

The study concerns the class of nonlinear Single-Input Single-Output (SISO) systems described by

$$\dot{y} = h(t, y) + g(t, y)u_0 + d(t) \quad (1)$$

where $y \in \mathbb{R}$ is available from measurements, the scalar functions $h(t, y), g(t, y) \in \mathcal{C}^1$ are bounded for bounded y , $g(t, y) \neq 0$, $\forall (t, y) \in [0, \infty) \times \mathbb{R}$ and $d(t) \in \mathcal{C}^2$ is a T -periodic unknown function. Such systems are frequently encountered in industrial applications that include repeated closed-curve tracking such as machine tool drive axes [21], where $d(t)$ could be the effect of Coulomb friction and cogging torques on the drive motor and axis dynamics that cause contouring deformations [22]. The control law

$$u_0 = g^{-1}(t, y) [-h(t, y) + u] \quad (2)$$

$$u = -k_1|y|^{\frac{1}{2}}\text{sgn}(y) - k_2 \int_0^t \text{sgn}(y(\tau))d\tau, \quad (3)$$

where $\text{sgn}(\cdot)$ is the signum function, gives the following second-order closed-loop dynamics

$$\underbrace{\begin{bmatrix} \dot{x}_1 \\ \dot{x}_2 \end{bmatrix}}_{\dot{\mathbf{x}}} = \underbrace{\begin{bmatrix} -k_1|x_1|^{\frac{1}{2}}\text{sgn}(x_1) + x_2 \\ -k_2\text{sgn}(x_1) + q(t) \end{bmatrix}}_{\mathbf{f}(t, \mathbf{x})}, \quad (4)$$

with $x_1 \triangleq y$, $x_2 \triangleq -k_2 \int_0^t \text{sgn}(y(\tau))d\tau + d(t)$ and $q(t) \triangleq \dot{d}(t)$. Since $d(t) \in \mathcal{C}^2$ and is T -periodic, it follows that its derivative is a continuous bounded T -periodic function. Let $|q(t)| \leq L$, where $L > 0$. It has been shown [12] that if

$$k_2 > L \quad (5)$$

$$k_1 \geq 1.8\sqrt{k_2 + L}, \quad (6)$$

then the system in (4) has a unique finite-time stable equilibrium point at the origin. The use of $\text{sgn}(y)$ implies infinitely fast switching of the control signal, which is not feasible in real-life control systems due to actuator limitations. In practice, the signum function is approximated by a continuous ‘‘boundary layer’’ function such as the following [23]

$$\phi_\delta(q, \delta) \triangleq \begin{cases} 1 & \text{if } q \geq \delta \\ \frac{q}{\delta} & \text{if } -\delta < q < \delta \\ -1 & \text{if } q \leq -\delta \end{cases}, \quad (7)$$

where δ is the width of the boundary layer. By doing so, the discontinuous vector field $\mathbf{f}(t, \mathbf{x})$ in (4) is *regularised*, i.e. is approximated by a continuous vector field, which often simplifies the analysis of the closed-loop system. It was proven in [20] that such an approximation can be made with arbitrarily large accuracy by letting $\delta \rightarrow 0$. The practical implication of this approximation is that results relating to convergence to the origin now correspond to convergence to a neighbourhood of the origin or arbitrarily small size (depending on δ). This is also what actually happens in real systems due to the effect of noise and other model inaccuracies. The regularised vector field will be considered in the entire subsequent analysis.

B. Existence and properties of limit cycles

Consider the regularised system $\dot{\mathbf{x}} = \mathbf{f}_\delta(t, \mathbf{x})$ with

$$\mathbf{f}_\delta(t, \mathbf{x}) \triangleq \begin{bmatrix} -k_1|x_1|^{\frac{1}{2}}\phi_\delta(x_1, \delta) + x_2 \\ -k_2\phi_\delta(x_1, \delta) + q(t) \end{bmatrix}, \quad (8)$$

where $k_1, k_2 > 0$, $k_2 < L$ and $\phi_\delta : \mathbb{R} \times (0, +\infty) \rightarrow [-1, 1]$ defined in (7). The following proposition states the conditions under which the boundedness of the regularised (and by extension of the real) system is ensured by means of convergence to a limit cycle even though the finite-time stability conditions do not hold ($k_2 < L$). Obviously, the size of the limit cycle along $x_1 = 0$, i.e. the bound on $x_1(t)$, is a metric for the closed-loop system accuracy.

Proposition 1 ([20]): Consider the closed-loop system (4) and its approximation associated with the regularisation (8), where $q(t)$ is Lipschitz, T -periodic of sufficiently small period T and $|q(t)| \leq L$. Then, $\exists \varepsilon_1 > 0$ with $0 < T < \varepsilon_1$ such that under the conditions

$$k_2 > \left| \frac{1}{T} \int_0^T q(t)dt \right| \quad (9)$$

$$k_1 \geq 1.8 \sqrt{k_2 + \left| \frac{1}{T} \int_0^T q(t)dt \right|} \quad (10)$$

the trajectories of the regularised system $\dot{\mathbf{x}} = \mathbf{f}_\delta(t, \mathbf{x})$ converge to a limit cycle with period T .

Proof: The regularised system can be written as

$$\dot{\mathbf{x}} = \varepsilon \frac{1}{T} \mathbf{f}_\delta(t, \mathbf{x}) \triangleq \varepsilon \mathbf{g}(t, \mathbf{x}), \quad \varepsilon = T, \quad (11)$$

where $\mathbf{g}(t, \mathbf{x})$ is Lipschitz continuous. The associated averaged system is written as

$$\dot{\boldsymbol{\chi}} = \varepsilon \bar{\mathbf{g}}(\boldsymbol{\chi}), \quad \boldsymbol{\chi} = [\chi_1 \quad \chi_2]^T \in \mathbb{R}^2 \quad (12)$$

with $\varepsilon \bar{\mathbf{g}}(\boldsymbol{\chi}) = \frac{1}{T} \int_0^T \mathbf{f}_\delta(t, \mathbf{x})dt$ and finally

$$\dot{\boldsymbol{\chi}} = \begin{bmatrix} -k_1|\chi_1|^{\frac{1}{2}}\phi_\delta(\chi_1, \delta) + \chi_2 \\ -k_2\phi_\delta(\chi_1, \delta) + \frac{1}{T} \int_0^T q(t)dt \end{bmatrix}. \quad (13)$$

Comparing (13) to (8) reveals that if conditions (9) and (10) hold, then for sufficiently small δ ($\delta \rightarrow 0$) the origin is a finite-time stable equilibrium point of the averaged system. Then, by Theorem 4.1.1 in [24], there exists $\varepsilon_1 > 0$, such that $\forall \varepsilon \in (0, \varepsilon_1)$, the solutions of (11) converge to a unique isolated T -periodic orbit $\gamma_\varepsilon(t) = O(\varepsilon)$ of same stability type. ■

The constant ε_1 relates to the largest time scale $\frac{1}{\varepsilon_1}$ for which approximation of the system dynamics via averaging is practically valid. Conditions (9) and (10) are much less strict than those for finite-time convergence since in case of symmetric perturbation rates ($\int_0^T q(t)dt = 0$), boundedness of the solutions is ensured by merely selecting positive gains irrespectively of how large the perturbation rate may be.

The remaining analysis concerns the size of the limit cycle, i.e. the bound on $x_1(t)$, and its relation to the perturbation

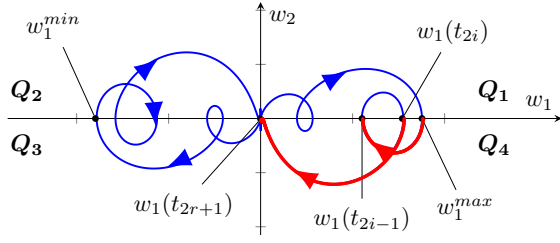


Fig. 1. One full period of the limit cycle.

characteristics and controller gains. To proceed with this analysis, it is convenient to express the closed-loop dynamics in the phase space coordinates $w_1 \triangleq x_1$ and $w_2 \triangleq \dot{x}_1$ as

$$\dot{w}_1 = w_2 \quad (14)$$

$$\dot{w}_2 = -\frac{1}{2}k_1|w_1|^{-\frac{1}{2}}w_2 - k_2\text{sgn}(w_1) + q(t). \quad (15)$$

Proposition 2 ([20]): After the trajectories of the closed-loop system converge to the limit cycle, the bound on the state x_1 varies proportionally to the perturbation bound L and to the square of the perturbation period T .

Proof: Let Q_j , $j = 1, \dots, 4$ be the four quadrants of the phase space and consider one period of the limit cycle as shown in Figure 1. For $t \geq t_0$ assume that the trajectories $w(t)$ intersect with semi-axis $w_1 \geq 0$ at $2r + 1$ points, $r \in \mathbb{N}$ starting from $w_1^{max} \triangleq w_1(t_0)$, which is the maximum value of $w_1(t)$. Since the trajectories cannot cross from Q_1 to Q_2 (due to increasing w_1), each trajectory segment that lies in Q_4 starting at an intersection point will have to either cross the semi-axis $w_1 \geq 0$ twice (one while crossing to Q_1 and one right after while crossing to Q_4) or cross the vertical axis towards Q_3 . In both cases, there will always be an odd number of intersections with the semi-axis $w_1 \geq 0$. Let these intersections occur at time instances t_{2i} (from Q_1 to Q_4) and t_{2i+1} (from Q_4 to Q_1), $i \in \mathcal{I} \triangleq \{0, \dots, r\}$ with $w(t)$ crossing from Q_4 to Q_3 at $t = t_{2r+1}$. In each time interval $[t_{2i}, t_{2i+1}]$, where $w_1(t) > 0$, $w_2(t) \leq 0$ holds (red lines):

$$\dot{w}_2(t) \geq -(k_2 + L) \Rightarrow w_2(t) \geq -(k_2 + L)(t - t_{2i}), \quad (16)$$

$\forall t \in (t_{2i}, t_{2i+1}]$ since $w_2(t_{2i}) = 0$. This leads to

$$\int_{t_{2i}}^{t_{2i+1}} w_2(t) dt > -\frac{1}{2}(k_2 + L)(t_{2i+1} - t_{2i})^2, \quad i \in \mathcal{I}.$$

Since $w_1(t_{2r+1}) = 0$ and $w_2(t) \geq 0$, $\forall t \in [t_{2i-1}, t_{2i}]$, $i \in \mathcal{I} - \{0\}$, it follows that

$$\begin{aligned} w_1^{max} &= -\left(\sum_{i=0}^r \int_{t_{2i}}^{t_{2i+1}} w_2(t) dt + \sum_{i=1}^r \int_{t_{2i-1}}^{t_{2i}} w_2(t) dt \right) \\ &\leq \frac{1}{2}(k_2 + L) \sum_{i=0}^r (t_{2i+1} - t_{2i})^2 \\ &< \frac{1}{2}(k_2 + L) \left(\sum_{i=0}^r (t_{2i+1} - t_{2i}) \right)^2 < \frac{1}{2}(k_2 + L)n^2T^2 \end{aligned}$$

given that $t_{2i+1} > t_{2i}$, $\forall i \in \mathcal{I}$ and $\sum_{i=0}^r (t_{2i+1} - t_{2i}) < t_{2r+1} - t_0 \leq nT$, $0 < n \leq \frac{1}{2}$. Due to the homogeneity of the STSMC closed-loop system [12], the same analysis in Q_2, Q_3

gives a similar result for the minimum value that x_1 assumes, which finally leads to

$$\max_{x(t) \in \gamma_\epsilon(t)} |x_1(t)| < \frac{1}{2}(k_2 + L)n^2T^2, \quad 0 < n \leq \frac{1}{2}. \quad (17)$$

The result in inequality (17) implies that faster perturbations have less effect on the accuracy bounds since they are “better averaged”, whereas, as expected, larger perturbations compromise accuracy. Moreover, from (16) it can be seen that too large value for the integral gain k_2 will result in faster changes in x_1 , i.e. in an increase of the induced chatter.

C. Tuning based on accuracy specifications

The description of the closed-loop dynamics in phase coordinates introduced in the previous section allows for a straightforward expression of the bound on $w_1(t) = x_1(t)$ as a function of the controller gains and, conversely, for an systematic tuning of the STSMC given a accuracy specification.

Consider again a full period of the limit cycle in Figure 1 restricted in Q_1 and the time interval $\mathcal{T} \triangleq [t_0, t_m]$, where t_0 is the time when the trajectories first enter Q_1 from Q_2 , $w_1(t_m) = w_1^{max} \geq w_1(t)$, $\forall t \in \mathcal{T}$ and the time instant $t^* \in \mathcal{T}$ such that $w_2(t^*) \geq w_2^*(t)$, $\forall t \in \mathcal{T}$. Integrating Equation (15) over the interval $[t_0, t_m]$, where $w_1(0) = 0$, $w_2(0) > 0$, $w_1(t_m) = w_1^{max}$, $w_2(t_m) = 0$ and $\dot{w}_2(t^*) = 0$ leads to

$$\begin{aligned} \int_0^{t_m} \dot{w}_2(t) dt &= \int_0^{t_m} (q(t) - k_2) dt - \int_0^{t_m} k_1 \frac{\dot{w}_1(t)}{2\sqrt{w_1(t)}} dt \\ &\Rightarrow -w_2(0) \leq -k_1\sqrt{w_1^{max}} + (L - k_2)t_m \Rightarrow \\ \sqrt{w_1^{max}} &\leq \frac{w_2(0) + (L - k_2)t_m}{k_1}. \end{aligned} \quad (18)$$

Evaluating Equation (15) at $t = t^*$ gives

$$w_2(t^*) = 2\frac{q(t^*) - k_2}{k_1} \sqrt{w_1(t^*)}. \quad (19)$$

Since $w_2(t^*) \geq w_2(t)$, $\forall t \in [t_0, t_m]$, Equation (19) yields

$$w_2(0) \leq w_2(t^*) \leq \frac{2(L - k_2)}{k_1} \sqrt{w_1^{max}}$$

and from (18) one obtains

$$\begin{aligned} \sqrt{w_1^{max}} &\leq \frac{\frac{2(L - k_2)}{k_1} \sqrt{w_1^{max}} + (L - k_2)t_m}{k_1} \Rightarrow \\ \frac{k_1^2 - 2(L - k_2)}{k_1} \sqrt{w_1^{max}} &\leq k_1(L - k_2)nT, \quad 0 < n \leq \frac{1}{2}, \end{aligned} \quad (20)$$

since $0 < t_m \leq \frac{T}{2}$. Finally, if k_1 is selected such that

$$k_1 > \sqrt{2(L - k_2)} \quad (21)$$

then a not overly conservative bound for w_1^{max} is given by

$$w_1^{max} \leq \frac{k_1^4(L - k_2)^2 n^2 T^2}{[k_1^2 - 2(L - k_2)]^2} \triangleq W_1(k_1, k_2). \quad (22)$$

Given an accuracy specification $|x_1(t)| \leq \eta$, k_1 and k_2 can be obtained by means of numerical optimisation or by selecting

TABLE I

REAL AND ESTIMATED ERROR BOUND IN CONSTANT SPEED REGIME.

ω_r (rad/s)	12	13	14	15	16	17
$\max e(t) $	0.182	0.170	0.161	0.156	0.157	0.128
w_1^{max}	0.565	0.482	0.415	0.362	0.318	0.282
ω_r (rad/s)	18	19	20	21	22	23
$\max e(t) $	0.141	0.129	0.115	0.114	0.099	0.112
w_1^{max}	0.251	0.226	0.204	0.185	0.168	0.154

one gain and solving for the other. This is often the case in electromechanical systems, where k_1 represents forces and currents delivered by the actuator and it is desired to keep the level of actuation below some rated values. In such case, fixing k_1 allows for calculating k_2 from (22):

$$k_2 \geq L - \frac{\sqrt{\eta}k_1^2}{2\sqrt{\eta} + k_1 n T} \quad (23)$$

III. EXPERIMENTAL VERIFICATION

This section presents the physical system and scenarios used for validating the theoretical findings of the previous sections and discusses the obtained results. The experimental setup comprised a commercial Siemens 1FT7042-5AF70 PMSM equipped with a SINAMICS S120 drive converter with 11-bit IC22DQ incremental angle encoder. The test scenarios covered two regimes of motion: constant speed and sinusoidal velocity profile. The total perturbation $d(t)$ acting on the motor is the sum of friction and cogging torques given by [25], [26]:

$$d(t) = T_C \frac{2}{\pi} \arctan(\alpha\omega) + \beta\omega + \sum_{i=1}^N F_i \sin(\theta + \psi_i) \quad (24)$$

$$\dot{d}(t) = \left[\frac{2T_C\alpha}{\pi(1 + \alpha^2\omega^2)} + \beta \right] \dot{\omega} + \omega \sum_{i=1}^N F_i \cos(\theta + \psi_i) \quad (25)$$

where ω, θ are the angular velocity and position of the motor, T_C, β are the Coulomb and viscous friction coefficients, $\alpha \gg 1$ is the steepness factor of the Coulomb friction model for approximating the signum function and F_i, ψ_i are the amplitude and phase offset of the cogging torque component related to the i^{th} harmonic. In all the experiments the signal of interest was the error $e \triangleq \omega - \omega_r$ and d, \dot{d} were estimated via robust differentiation of the measured velocity and control input u as $d = J\dot{\omega} - u$, where J is the motor inertia.

A. Speed regulation at constant set-point

While the motor operates at almost constant angular velocity ω_r , then $\dot{\omega} \cong 0$ and from (25) one gets $|\dot{d}(t)| \leq \left| \omega_r \sum_{i=1}^N F_i \right| \triangleq L$. Moreover, the period of $d(t)$ is approximately given by $T = 2\pi/\omega_r$. A total number of 12 experiments with constant speed set-points $\omega_r \in \{12, 13, \dots, 23\}$ rad/s were carried out to assess the validity of the theoretical

TABLE II

REAL AND ESTIMATED ERROR BOUND FOR SINUSOIDAL VELOCITY.

f (Hz)	1	1.5	2	2.5	3	3.5	4	5
$\max e(t) $	0.174	0.143	0.127	0.117	0.126	0.123	0.119	0.11
w_1^{max}	3.063	1.361	0.766	0.49	0.34	0.25	0.191	0.123

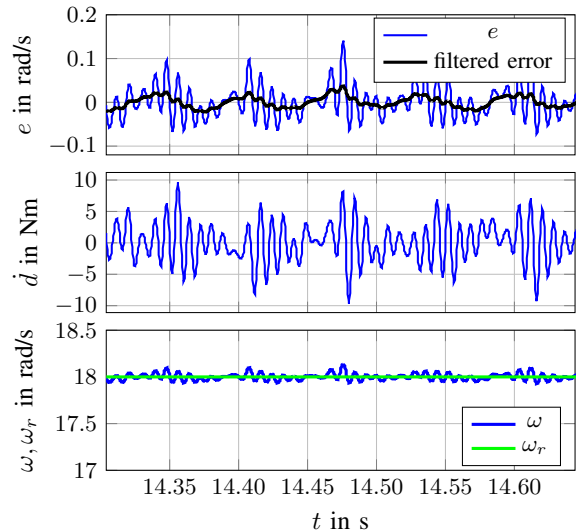


Fig. 2. Error, disturbance rate and motor velocity for reference $\omega_r = 18$ rad/s. The periodicity of the error matches this of the perturbation rate.

results. It was not possible to keep constant perturbation rate amplitude for all the experiments since both ω_r and the harmonics amplitudes F_i were varying at different frequencies of operation. It was, however, observed that L ranged from approximately 8 to 11 Nm/s and never exceeded 12 Nm/s, whereas its mean value over a single period was approximately 0. The finite-time convergence gains were calculated from (5),(6) as $\bar{k}_1 = 9.1$ and $\bar{k}_2 = 13.2$. The gains applied to the system were selected as $k_1 = 0.9$ and $k_2 = 11.65 < L$ according to (23) for $\eta = 0.2$ rad/s. Figure 5 illustrates the phase plots for all the experiments with constant speed. As it can be seen, the closed-loop trajectories converge to a limit cycle. Figure 2 that shows the time responses of e, \dot{d} and ω during a full period for $\omega_r = 18$ rad/s, reveals that the signals have the same periodicity as predicted from the theoretical analysis. For increasing perturbation frequency, the actual error bound quadratically decreased as also shown in the bottom Figure 4. Finally, Table I shows a comparison between the real error bound and the one estimated based on (17) with $n = 0.5$.

B. Tracking of sinusoidal velocity reference

Eight experiments with different sinusoidal velocity references at frequencies $f_i \in \{1, 1.5, \dots, 4, 5\}$ Hz were carried out for testing the STSMC closed-loop behaviour during motion reversals. Choosing $\omega_r(t) = \frac{100}{2\pi f_i} \cos(2\pi f_i t)$ ensured constant acceleration peak for all f_i . In this case the friction rate assumed its highest magnitude $100 \left(\frac{2T_C\alpha}{\pi} + \beta \right)$ for zero

velocity, where the contribution from the cogging torques was zero. For maximum velocity, the friction contribution was very small, whereas that of the cogging torques was the dominant one. In all experiments L was no larger than 20 Nm/s. The finite-time convergence gains were calculated as $\bar{k}_1 = 10.5$ and $\bar{k}_2 = 22$, while the actual gains were selected as $k_1 = 0.9$ and $k_2 = 19.65$ according to (23) for the same accuracy specification $\eta = 0.2$ rad/s. Again, the velocity error trajectory was periodic with same periodicity as the perturbation rate as seen in Figure 3. The associated phase plots in Figure 6 illustrating the limit cycles showed decreasing error bound for increasing perturbation frequency f . This is more clearly seen in the top Figure 4 where a reciprocal quadratic relation is observed between f and the error bound. Similarly to the constant speed experiments, Table II shows the comparison between the real error bound and the one estimated based on (17) with $n = 0.5$.

IV. CONCLUSIONS

Experimental validation of the stability properties of under-tuned super-twisting sliding mode control loops under the effect of periodic perturbations was pursued in this paper. Based on a series of tests performed on a commercial industrial motor, it was demonstrated that the existence of a limit cycle of the same period as the perturbation can be guaranteed under milder controller gain conditions compared to those required for finite-time stability. The experimental results verified that the width of the limit cycle quadratically decreases for smaller perturbation periods. Moreover, the controller gains provided by the proposed tuning guidelines were successfully applied to the real system ensuring that the considered accuracy specifications were satisfied. Future work will focus on reducing the conservatism in estimating the accuracy bounds in terms of both the perturbation profile and in relation to estimating the period fraction n .

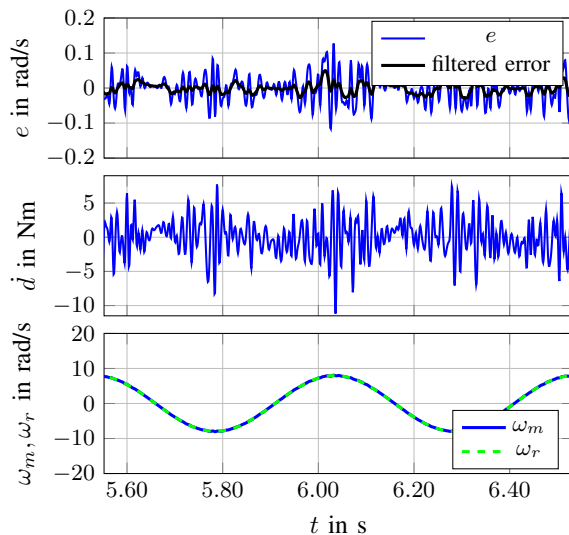


Fig. 3. Error, disturbance rate and motor velocity for sinusoidal reference at 2 Hz. The periodicity of the error matches this of the perturbation rate.

REFERENCES

- [1] S. V. Emelyanov, "Variable structure control systems," *Moscow, Nauka*, 1967.
- [2] Y. Shtessel, J. Buffington, and S. Banda, "Tailless aircraft flight control using multiple time scale reconfigurable sliding modes," *IEEE Transactions on Control Systems Technology*, vol. 10, no. 2, pp. 288–296, 2002.
- [3] V. Utkin, J. Guldner, and J. Shi, *Sliding mode control in electro-mechanical systems*. CRC press, 2017.
- [4] C. Edwards, S. K. Spurgeon, and R. J. Patton, "Sliding mode observers for fault detection and isolation," *Automatica*, vol. 36, pp. 541–553, 2000.
- [5] G. Bartolini, A. Ferrara, and E. Usai, "Chattering avoidance by second-order sliding mode control," *IEEE Transactions on Automatic Control*, vol. 43, no. 2, pp. 241–246, 1998.
- [6] A. Levant, "Homogeneity approach to high-order sliding mode design," *Automatica*, vol. 41, no. 5, pp. 823–830, 2005.
- [7] —, "Sliding order and sliding accuracy in sliding mode control," *International Journal of Control*, vol. 58, no. 6, pp. 1247–1263, 1993.
- [8] H. Haimovich and H. De Battista, "Disturbance-tailored super-twisting algorithms: Properties and design framework," *Automatica*, vol. 101, pp. 318–329, 2019.
- [9] A. Levant, "Principles of 2-sliding mode design," *Automatica*, vol. 43, no. 4, pp. 576 – 586, 2007.
- [10] J. A. Moreno and M. Osorio, "Strict lyapunov functions for the super-twisting algorithm," *IEEE Transactions on Automatic Control*, vol. 57, no. 4, pp. 1035–1040, 2012.
- [11] A. K. Behera, A. Chalanga, and B. Bandyopadhyay, "A new geometric proof of super-twisting control with actuator saturation," *Automatica*, vol. 87, pp. 437–441, 2018.
- [12] R. Seeber and M. Horn, "Necessary and sufficient stability criterion for the super-twisting algorithm," *Proceedings of IEEE International Workshop on Variable Structure Systems*, vol. 2018-, pp. 8460445, 120–125, 2018.
- [13] R. Seeber, M. Horn, and L. Fridman, "A novel method to estimate the reaching time of the super-twisting algorithm," *IEEE Transactions on Automatic Control*, vol. 63, no. 12, p. 8307188, 2018.
- [14] A. Piloni, A. Pisano, and E. Usai, "Parameter tuning and chattering adjustment of super-twisting sliding mode control system for linear plants," *Proceedings of Ieee International Workshop on Variable Structure Systems*, pp. 6163549, 479–484, 2012.
- [15] Y. Shtessel, M. Taleb, and F. Plestan, "A novel adaptive-gain super-twisting sliding mode controller: Methodology and application," *Automatica*, vol. 48, no. 5, pp. 759–769, 2012.

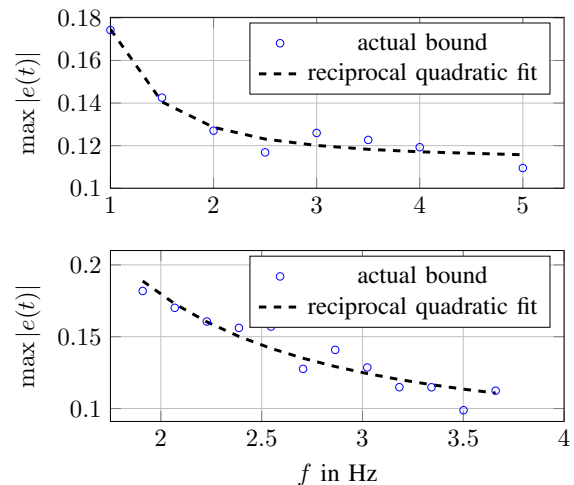


Fig. 4. Velocity error bound as a function of the perturbation frequency f for sinusoidal velocity reference (top) and constant velocity reference (bottom). In both cases, the error shows a quadratic decrease with respect to the frequency.

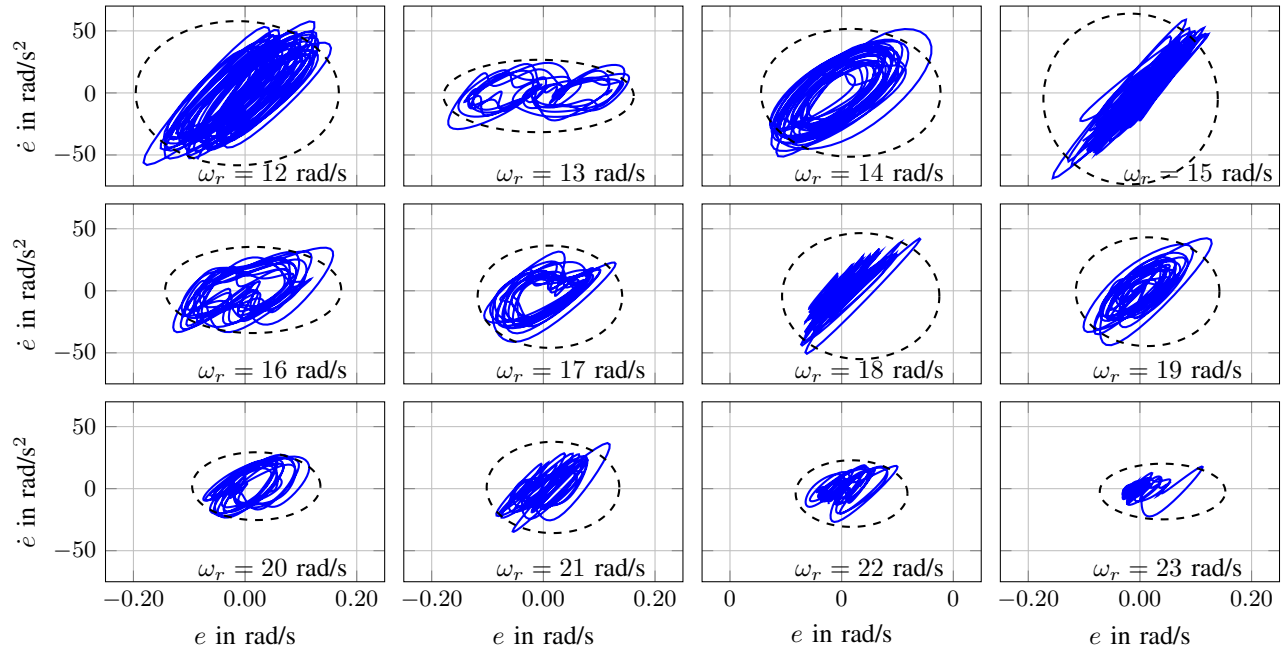


Fig. 5. Phase plots for constant velocity reference ω_r . The enclosing ellipse is drawn to highlight the decrease of the width of the limit cycles for increasing frequency of the perturbation.

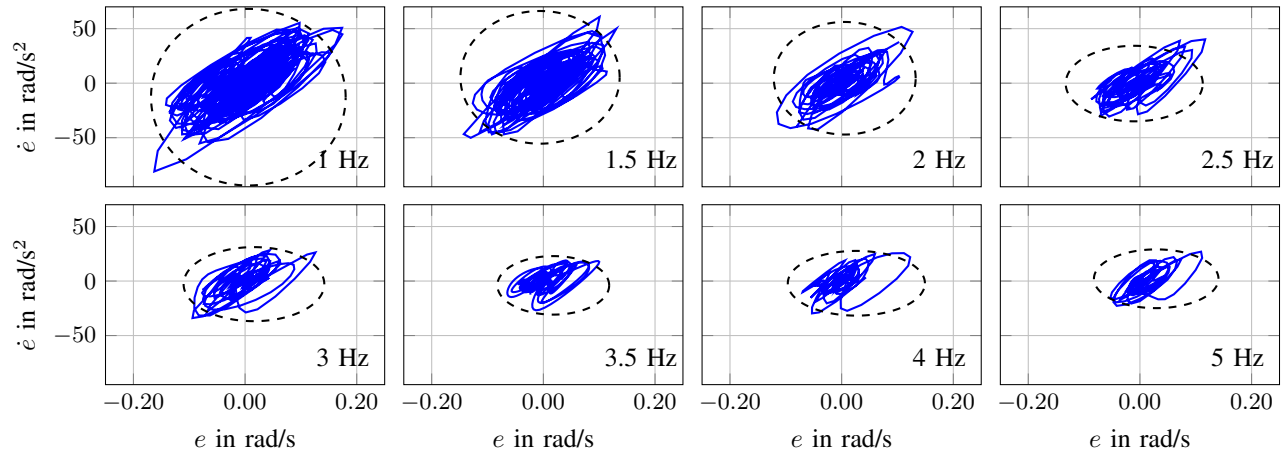


Fig. 6. Phase plots for sinusoidal velocity reference $\omega_r(t) = \frac{100}{2\pi f_i} \cos(2\pi f_i t)$. The enclosing ellipse is drawn to highlight the decrease of the width of the limit cycles for increasing frequency of the perturbation.

- [16] A. Barth, M. Reichhartinger, J. Reger, M. Horn, and K. Wulff, "Lyapunov-design for a super-twisting sliding-mode controller using the certainty-equivalence principle," *IFAC-papersonline*, vol. 28, no. 11, pp. 860–865, 2015.
- [17] C. Edwards and Y. B. Shtessel, "Adaptive continuous higher order sliding mode control," *Automatica*, vol. 65, pp. 183–190, 2016.
- [18] C. Edwards and Y. Shtessel, "Adaptive dual-layer super-twisting control and observation," *International Journal of Control*, vol. 89, no. 9, pp. 1759–1766, 2016.
- [19] D. Papageorgiou, M. Blanke, H. H. Niemann, and J. H. Richter, "Adaptive and sliding mode friction-resilient machine tool positioning—cascaded control revisited," *Mechanical Systems and Signal Processing*, vol. 132, pp. 35–54, 2019.
- [20] D. Papageorgiou and C. Edwards, "On the behaviour of under-tuned super-twisting sliding mode control loops," *Automatica*, vol. 135, p. 109983, 2022.
- [21] Y. Altintas, *Manufacturing Automation: Metal Cutting Mechanics, Machine Tool Vibrations, and CNC Design*, 2nd ed. Cambridge University Press, 2012.
- [22] H. Gross, J. Hamann, and G. Wiegärtner, *Electrical feed drives in automation: basics, computation, dimensioning*. Publicis, 2001.
- [23] J. Llibre, D. D. Novaes, and M. A. Teixeira, "On the birth of limit cycles for non-smooth dynamical systems," *Bulletin des Sciences Mathématiques*, vol. 139, no. 3, pp. 229–244, 2015.
- [24] J. Guckenheimer and P. Holmes, *Nonlinear Oscillations, Dynamical Systems, and Bifurcations of Vector Fields*. Springer, 1983, vol. 42.
- [25] D. Papageorgiou, M. Blanke, H. Henrik Niemann, and J. H. Richter, "Online friction parameter estimation for machine tools," *Advanced Control for Applications: Engineering and Industrial Systems*, vol. 2, no. 1, p. e28, 2020.
- [26] M. Lukaniszyn, M. Jagiela, and R. Wrobel, "Optimization of permanent magnet shape for minimum cogging torque using a genetic algorithm," *IEEE Transactions on Magnetics*, vol. 40, no. 2, pp. 1228–1231, 2004.